

# UniEmo: Unifying Emotional Understanding and Generation with Learnable Expert Queries

Yijie Zhu, Lingsen Zhang, Zitong Yu<sup>†</sup>, *Senior Member, IEEE*, Rui Shao<sup>†</sup>, *Member, IEEE*, Tao Tan, *Member, IEEE*, Liqiang Nie *Senior Member, IEEE*

**Abstract**—Emotional understanding and generation are often treated as separate tasks, yet they are inherently complementary and can mutually enhance each other. In this paper, we propose the UniEmo, a unified framework that seamlessly integrates these two tasks. The key challenge lies in the abstract nature of emotions, necessitating the extraction of visual representations beneficial for both tasks. To address this, we propose a hierarchical emotional understanding chain with learnable expert queries that progressively extracts multi-scale emotional features, thereby serving as a foundational step for unification. Simultaneously, we fuse these expert queries and emotional representations to guide the diffusion model in generating emotion-evoking images. To enhance the diversity and fidelity of the generated emotional images, we further introduce the emotional correlation coefficient and emotional condition loss into the fusion process. This step facilitates fusion and alignment for emotional generation guided by the understanding. In turn, we demonstrate that joint training allows the generation component to provide implicit feedback to the understanding part. Furthermore, we propose a novel data filtering algorithm to select high-quality and diverse emotional images generated by the well-trained model, which explicitly feedback into the understanding part. Together, these generation-driven dual feedback processes enhance the model’s understanding capacity. Extensive experiments show that UniEmo significantly outperforms state-of-the-art methods in both emotional understanding and generation tasks. The code for the proposed method is available at <https://github.com/JiuTian-VL/UniEmo>

**Index Terms**—Visual emotion understanding, visual emotion generation, cross-task feedback, emotion-conditioned synthesis.

## I. INTRODUCTION

Emotional understanding has gained significant attention due to its crucial role in various domains such as human-computer interaction [1], [2], [3], [4], [5], mental health [6] and entertainment [7], [8]. Existing approaches [9], [10], [11], [12], [13], [14], [15] treat visual emotion understanding as a conventional classification task, as illustrated in Fig. 1(a). Typically, a visual encoder extracts features, which are then mapped to target emotion using a classification head.

Beyond emotional understanding, Emotional Image Content Generation (EICG) has emerged as a key research direction [16]. This generative task is particularly valuable in digital media, virtual environments, and marketing [17], [18], [19]. Current works commonly create a latent emotion space in

which similar emotional representations are grouped closely, while dissimilar ones are separated. To generate an image that embodies a specific emotion, the corresponding emotional feature extracted from this latent space is used as a conditioning input to guide the diffusion model [20], [21], [22], [23], [24], as shown in Fig. 1(b).

Although emotional understanding and generation are generally treated as separate tasks, they are inherently complementary [25], [26], [27], [28]. Enhancing emotional generation depends on a deeper emotional understanding [16], as a better comprehension of emotional cues leads to more expressive image generation. Meanwhile, emotional generation can enhance emotional understanding by expanding limited emotion datasets with diverse, synthesized data [29]. Additionally, it provides generative feedback that refines distinctive emotional features, further enhancing emotional understanding [30].

Motivated by this synergy, we aim to design a unified framework that integrates them, enabling mutual reinforcement between the two tasks. To facilitate this integration, it is essential to identify a pivotal entry point. The core pipelines in existing methods, as depicted in Fig. 1(a) and (b), reveal that extracting emotion-relevant and semantically rich visual representations is essential for both tasks, which is the key to unify them. Specifically, a more accurate understanding of the emotional content in images requires richer emotional representations. Meanwhile, these representations can reinforce a more nuanced emotion space, which helps produce higher-quality emotional images. To extract such richer emotional representations, we need a more fine-grained emotional understanding capability. Building upon this, instead of focusing solely on advanced feature extractors [12], [13], [14], we propose decomposing the abstract emotional understanding process into a hierarchical visual chain. It starts with scene-level information, followed by object identification, both of which are crucial for emotion recognition [14], [31], [32], and then leverages these multi-scale prior features to infer emotions.

Building on the aforementioned ideas, we introduce two sets of learnable expert queries to extract hierarchical rich representations, thereby constructing a unified emotion understanding and generation framework based on them. Specifically, there are three key steps to build such a framework: **1) Hierarchical Emotional Understanding Chain with Expert Queries**. The two sets of expert queries serve different purposes: one set focuses on extracting scene-level features, while the other targets object-level features. As illustrated by the blue section in Fig. 1(c), they are progressively integrated into the network

<sup>†</sup> Corresponding author: Zitong Yu (email: yuzitong@gbu.edu.cn) and Rui Shao (email: shaorui@hit.edu.cn).

Yijie Zhu is with Harbin Institute of Technology, Shenzhen, Shenzhen 518055, China, and Great Bay University, Dongguan 523000, China.

Lingsen Zhang, Rui Shao, and Liqiang Nie are with Harbin Institute of Technology, Shenzhen, Shenzhen 518055, China.

Zitong Yu is with Great Bay University, Dongguan 523000, China.

Tao Tan is with Macao Polytechnic University, Macao 999078, China.

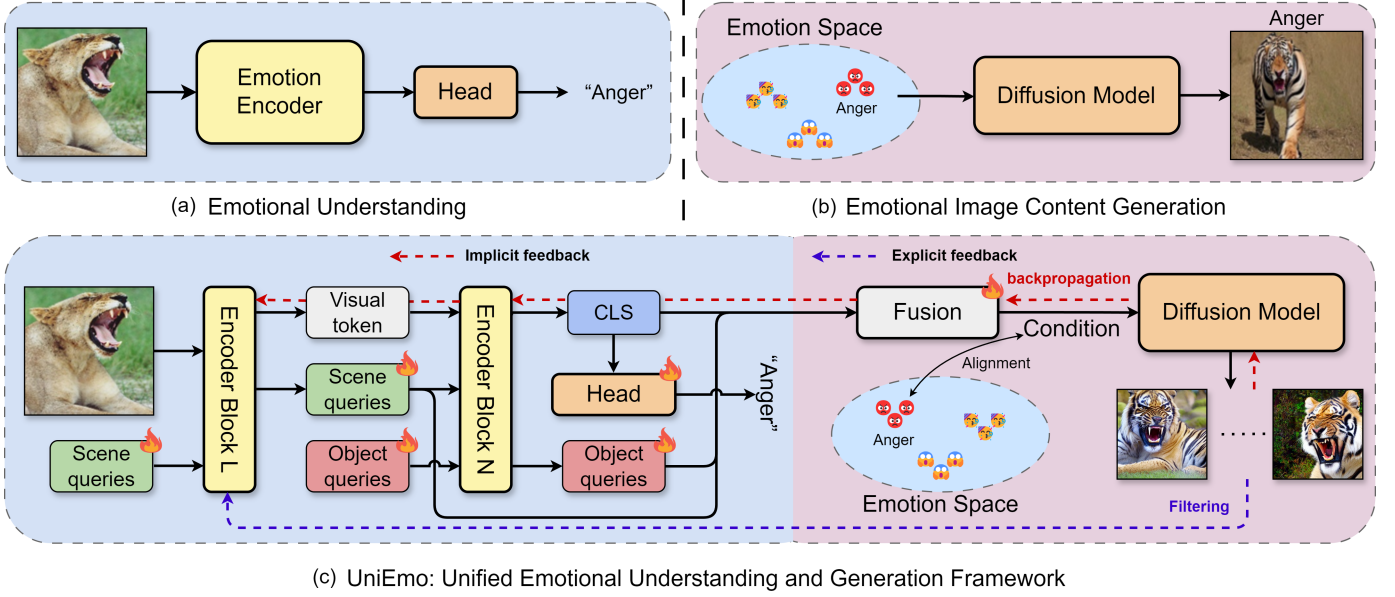


Fig. 1: The pipelines for existing methods focused on Emotional Understanding and Emotional Image Content Generation are shown in (a) and (b), respectively. In contrast, (c) illustrates our unified framework, **UniEmo**, which integrates both tasks. This framework comprises **three key steps**: the blue section indicates the first step, the pink section corresponds to the second step, and the dashed lines represent the third step. Detailed explanations of these steps are provided in the introduction.

to extract hierarchically rich emotional representations. 2) **Understanding-Guided Fusion and Alignment for Emotional Generation.** To condition the diffusion model for generating emotionally distinct and diverse images, we fuse these expert queries with emotional representations, as depicted by the pink section in Fig. 1(c). However, simple fusion risks weakening emotional signals and misaligning representations with the target emotion space. To address these issues, we introduce an emotional correlation coefficient to quantify the emotional relevance of expert queries and an emotional condition loss to align outputs with the target emotion space using contrastive learning. 3) **Generation-Driven Dual Feedback for Enhanced Emotional Understanding.** We demonstrate that joint training enables the generation component to provide implicit feedback that optimizes discriminative emotional representations and enhances understanding [30]. Additionally, we propose a novel data filtering algorithm to select high-quality and diverse emotional images generated by the well-trained model. By enriching the limited emotion dataset with such synthesized examples, this process provides explicit feedback to further strengthen the model’s understanding ability. The two types of feedback are represented by dashed lines in Fig. 1(c). In summary, our contributions are as follows:

- We introduce **UniEmo**, a novel framework that integrates emotional understanding and generation through a **hierarchical sequence of learnable expert queries**. These queries enable the progressive extraction of rich emotional features, forming the foundation for unification.
- We propose the **emotional correlation coefficient** for efficient fusion and design an **emotional condition loss** to align the fused features with the target emotion space, enhancing the quality of generated emotional images.

- We demonstrate that through joint training, the generation component provides **implicit feedback** to the understanding. Additionally, we propose a novel data filtering algorithm that **explicitly feeds back** into the understanding component, further enhancing performance.
- We conduct extensive experiments to validate UniEmo, demonstrating its superior performance in both emotional understanding and generation tasks.

## II. RELATED WORK

### A. Visual Emotion Understanding

Visual emotion understanding has attracted increasing attention in recent years [33]. Early approaches primarily relied on low-level visual features such as color, texture, and shape to infer emotional states [34], [35], [36]. With the advent of deep learning, convolutional neural networks (CNNs) have enabled the automatic learning of hierarchical features, ranging from edges and textures to complex shapes and patterns [37], [38], [7], thereby capturing nuanced emotional expressions beyond pixel-level details. Despite these advancements, many recent studies [39], [40], [10], [41] continue to focus primarily on enhancing visual feature extraction through increasingly complex neural architectures. Importantly, a growing body of evidence highlights the crucial role of high-level semantic concepts, such as scene context, salient objects, and their interactions, in shaping emotional perception [14], [31], [32].

To address these limitations, recent methods have started to incorporate structured semantic priors and auxiliary information. However, a systematic framework for modeling emotional understanding through multi-scale semantic reasoning is still lacking. To bridge this gap, our approach explicitly integrates scene-level and object-level representations via hierarchical

expert queries, which have been validated to offer complementary and discriminative cues for robust emotion recognition.

### B. Visual Emotion Generation

Visual emotion generation aims to synthesize visual content that evokes specific emotions by leveraging advanced generative models and affective computing techniques. Recently, diffusion models have achieved remarkable progress, giving rise to powerful frameworks such as GLIDE [42], DALL-E2 [43], eDiff-I [44], and Imagen [45]. These models excel at generating concrete concepts [22], [23], [46] and personalized imagery [47], [24], [48], but often struggle with producing abstract, emotion-evoking visuals.

To address this challenge, EmoGen [16] introduces an emotion space aligned with CLIP semantics [49], [21], [50] to enhance the emotional expressiveness of generated content. Similarly, EmoEdit [51] employs a vision-language model to identify emotion-relevant semantic factors and guides the generative model to modify images accordingly. EmotionPrompt[52] formulates emotional intent as learnable soft prompts, enabling emotion-conditioned generation by adapting the internal attention flow of diffusion models. EmotiCrafter[53] proposes a framework that models continuous affective dimensions—such as valence and arousal—and integrates them into the diffusion process to generate emotionally vivid and nuanced content.

### C. Query-Based Methods

Query-based mechanisms [54], [55], [56], [57], [58] have gained increasing attention in visual representation learning for their ability to decouple task-specific information extraction from raw image features. DETR [59] introduces object queries within a Transformer architecture to detect and localize physical entities, optimized through bipartite matching. Slot Attention [60] formulates unsupervised scene decomposition as an iterative querying process, where each slot learns to attend to a distinct object-like component. Subsequent works such as ViTDet [61] and DINO [62] extend this paradigm for object detection and dense prediction using query-based Transformer designs. In the vision-language domain, approaches like MaskCLIP [63] and DenseCLIP [64] employ language-driven prompts or queries to guide fine-grained semantic alignment between textual concepts and visual regions.

While these methods are effective for object detection and semantic alignment, they largely neglect abstract emotional semantics. In contrast, our approach introduces hierarchical expert queries—scene-level and object-level—specifically designed for emotional understanding and generation. This design is motivated by prior evidence highlighting the critical role of scenes and objects in emotion perception. Moreover, UniEmo employs a closed-loop framework where expert queries facilitate both recognition and generation, enabling synergistic learning and feedback across tasks.

## III. METHODOLOGY

In this section, we provide a detailed explanation of UniEmo. As shown in Fig. 1, the model operates within a closed-loop framework built around three key components:

1) a hierarchical emotional understanding chain with expert queries (blue section), 2) efficient fusion and alignment with these expert queries for emotional generation (pink section), and 3) dual feedback from the generation to the understanding (dashed lines). We will elaborate on these components sequentially in Secs. III-A–III-C.

### A. Hierarchical Emotional Understanding Chain with Expert Queries

For an input emotional image, we adopt the ViT [65] approach by dividing it into non-overlapping patches, linearly projecting them into patch tokens, and prepending a class token to the sequence. For convenience, in an  $N$ -layer ViT model, the class and patch tokens output from the  $m$ -th layer are denoted as  $T_m^{\text{Cls}}$  and  $T_m^{\text{Patch}}$  ( $0 \leq m \leq N$ ), respectively. Notably,  $T_0^{\text{Cls}}$  and  $T_0^{\text{Patch}}$  represent the input tokens before the first encoding layer.

**Multi-stage Expert Queries.** Instead of directly feeding the tokens into the forward pass to infer abstract emotions, we introduce two sets of learnable expert queries that decompose this process into a hierarchical visual chain. As shown in Fig. 2, the two expert queries, denoted as  $Q_m^{\text{Scene}}$  and  $Q_m^{\text{Object}}$ , are a series of learnable tokens designed to extract scene-level and object-level features, respectively. We divide the  $N$ -layer Transformer architecture into three hierarchical stages: layers 1 to  $L_1$ ,  $L_1 + 1$  to  $L_2$ , and  $L_2 + 1$  to  $N$ . Beginning with the first layer, we initially concatenate the  $T_0^{\text{Cls}}$ ,  $T_0^{\text{Patch}}$  and  $Q_0^{\text{Scene}}$ , and then pass them through the encoder layers from 1 to  $L_1$ , represented as:

$$[T_{L_1}^{\text{Cls}}, T_{L_1}^{\text{Patch}}, Q_{L_1}^{\text{Scene}}] = E_{1:L_1}([T_0^{\text{Cls}}, T_0^{\text{Patch}}, Q_0^{\text{Scene}}]), \quad (1)$$

where  $E_{1:L_1}$  denotes the Transformer encoder block from layer 1 to  $L_1$ ,  $[\cdot, \cdot]$  represents concatenation operation along the sequence dimension. The previous steps established an initial correlation between the expert query and image tokens. To strengthen this interaction, we introduce an Interactive Block, which facilitates the extraction of more detailed scene features from the image tokens. Specifically, this block functions as a compact transformer-style network with two layers, each comprising a multi-head attention mechanism, represented as  $A$ , followed by a feed-forward network, denoted as  $F$ . We input  $Q_{L_1}^{\text{Scene}}$  and  $T_{L_1}^{\text{Patch}}$  into the Interactive Block, with the computation process defined as:

$$\begin{aligned} \tilde{Q}_{L_1}^{\text{Scene}} &= Q_{L_1}^{\text{Scene}} + A(Q_{L_1}^{\text{Scene}}, T_{L_1}^{\text{Patch}}), \\ \tilde{Q}_{L_1}^{\text{Scene}} &= \tilde{Q}_{L_1}^{\text{Scene}} + F(\tilde{Q}_{L_1}^{\text{Scene}}). \end{aligned} \quad (2)$$

Subsequently, we enhance the original  $Q_{L_1}^{\text{Scene}}$  using the refined  $\tilde{Q}_{L_1}^{\text{Scene}}$ , which is derived from the output of the Interactive Block, following the procedure outlined below:

$$\hat{Q}_{L_1}^{\text{Scene}} = Q_{L_1}^{\text{Scene}} + \beta \tilde{Q}_{L_1}^{\text{Scene}}, \quad (3)$$

where  $\beta$  represents the learnable modulation parameter, enabling the model to effectively balance the contributions of both the primary and refined scene-level expert query.

To guide the expert query in extracting scene-level representations from emotional images, we use a contrastive loss to enforce semantic supervision and alignment. As illustrated in Fig. 2, for an example of a lion image, we use a CLIP [49]

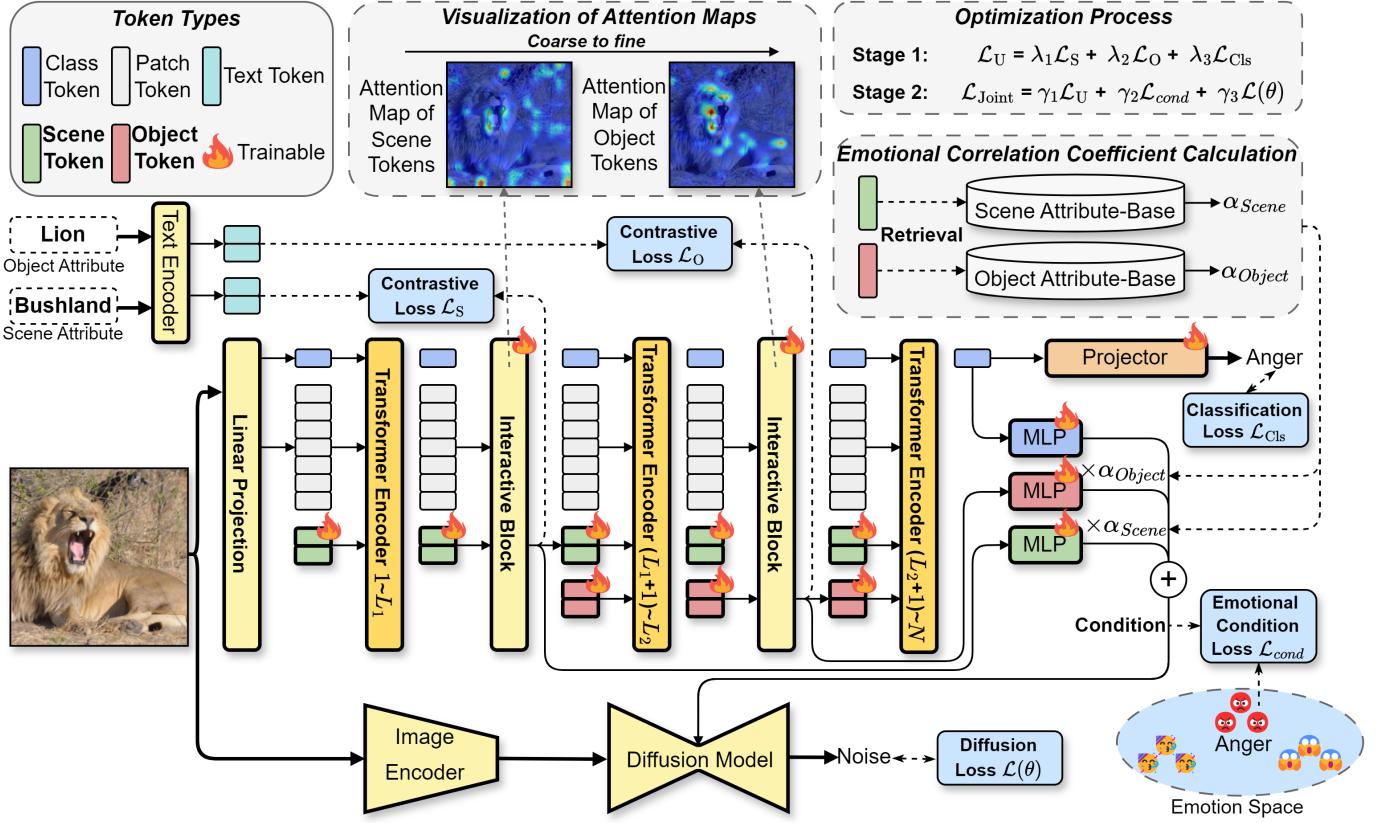


Fig. 2: Overview of our **UniEmo** framework, which leverages **two sets of learnable expert queries (scene tokens and object tokens)** to capture hierarchical emotional representations (step 1 mentioned in the introduction). These tokens and emotional representations are fused with **emotional correlation coefficients**  $\alpha_{\text{Scene}}$  and  $\alpha_{\text{Object}}$ , supervised by the **emotional condition loss**  $L_{\text{cond}}$  to guide the diffusion model in emotion-driven generation (step 2). Similar to Fig. 1(c), the generation component provides **dual feedback** to the understanding module, though this is not explicitly shown in this figure (step 3). The top section of the figure shows the attention maps for the expert queries.

text transformer to encode the corresponding scene attribute “bushland” as the supervisory signal. Formally, given a batch of  $K$  query-attribute pairs  $\{(\hat{Q}_{L_1,i}^{\text{Scene}}, z_i^{\text{Scene}})\}_{i=1}^K$ , where  $z_i^{\text{Scene}}$  represents the text embedding of corresponding scene attribute for the  $i$ -th pair, the contrastive loss  $\mathcal{L}_S$  is thus defined as:

$$\mathcal{L}_S = -\frac{1}{K} \sum_{i=1}^K \log \frac{\exp(\text{sim}(\hat{Q}_{L_1,i}^{\text{Scene}}, z_i^{\text{Scene}}) / \tau)}{\sum_{j=1}^K \exp(\text{sim}(\hat{Q}_{L_1,i}^{\text{Scene}}, z_j^{\text{Scene}}) / \tau)}, \quad (4)$$

where  $\text{sim}(\cdot, \cdot)$  denotes the dot product similarity, and  $\tau$  is a temperature hyperparameter, which is set to 0.07. Following the procedures outlined above, we enable the model to form an initial understanding of the global context of the entire image. Building on this prior, we introduce another expert query dedicated to extracting object-level features. Specifically, we concatenate the  $T_{L_1}^{\text{Cls}}$ ,  $T_{L_1}^{\text{Patch}}$ ,  $\hat{Q}_{L_1}^{\text{Scene}}$  and  $Q_{L_1}^{\text{Object}}$  at the input of layer  $L_1 + 1$ . Similar to the previous process, they are then passed through Transformer encoders from  $L_1 + 1$  to  $L_2$ , after which  $Q_{L_2}^{\text{Object}}$  and  $T_{L_2}^{\text{Patch}}$  are input into the Interactive Block. Object attributes encoded by the text encoder guide this process, producing a contrastive loss  $\mathcal{L}_O$ . Finally, the two sets of expert queries work together in the encoding layers from  $L_2 + 1$  to  $N$ . Thus, a hierarchical visual chain emerges, enabling a novel emotional understanding process that identifies abstract emotions and extracts multi-scale fea-

tures for unification. Notably, scene and object attributes are used solely during training to supervise expert query learning. Once trained, the model requires only a single image at inference time to perform emotion prediction.

### B. Understanding-Guided Fusion and Alignment for Emotional Generation

From the emotional understanding chain, we observe that the class token before the classification head encodes distinct emotional representations, while multi-stage expert queries capture diverse semantic features. By complementing these two components to form a clear and diverse emotion space [16], we can better guide the diffusion model to generate emotionally distinct and diverse images. However, multi-stage expert queries span a hierarchical spectrum of scene and object characteristics whose emotional valence can vary significantly. Some elements exhibit strong emotional resonance (e.g., Ferris wheels with amusement or flames with anger), while others are emotionally neutral (e.g., trees and grass). To address this variability, we propose an emotional correlation coefficient to quantitatively evaluate the relationship between expert queries and emotions. This coefficient is a pivotal metric for assessing the significance of these queries in the fusion process.

**Emotional Correlation Coefficient.** As shown in Fig. 3, we consolidate all scene and object attributes from the dataset





coefficients, which are set to 0.25, 0.25, and 0.5, respectively. In the second stage, we jointly train the two tasks:

$$\mathcal{L}_{\text{Joint}} = \gamma_1 \mathcal{L}_U + \gamma_2 \mathcal{L}_{\text{cond}} + \gamma_3 \mathcal{L}(\theta), \quad (10)$$

where the total loss  $\mathcal{L}_{\text{Joint}}$  incorporates  $\mathcal{L}_U$  from the first stage, alongside the emotional condition loss  $\mathcal{L}_{\text{cond}}$  and the diffusion loss  $\mathcal{L}(\theta)$ . The tuning coefficients  $\gamma_1$ ,  $\gamma_2$ , and  $\gamma_3$  are introduced to balance the contributions of these components during joint training, and are set to 0.3, 0.3, and 0.4, respectively. Our experimental observation indicates that joint training allows the generative component to implicitly provide feedback to enhance the understanding module.

**Explicit Feedback.** Meanwhile, we note that the model trained in the second stage demonstrates strong generative capabilities. To leverage this, we design an efficient data filtering algorithm to select high-quality emotional images. The filtered data are subsequently used to train the model, establishing an explicit feedback loop that complements the implicit feedback from the generation component. As shown in Alg. 1, to ensure emotional relevance and semantic clarity in the generated images, we employ Emo-A and Sem-C as evaluation criteria for filtering. Specifically, Emo-A verifies that each image conveys the intended emotional state, while Sem-C preserves clear, recognizable content, preventing the images from becoming overly abstract or indistinct. Detailed definitions of these metrics are provided in the experimental section. By selecting images within the top  $\eta\%$  to  $\delta\%$  range for both metrics, we achieve a balance between emotional expressiveness and semantic clarity. This dual constraint ensures that only the highest quality images, which effectively evoke emotions while remaining semantically interpretable, are retained for further training.

---

**Algorithm 1** Dual Metric High-Quality Image Filtering

---

**Require:** generated image set  $\mathcal{I}$ , CLIP model  $M_{\text{CLIP}}$ ,  
emotion classifier  $M_{\text{emo}}$ , thresholds  $\eta$ ,  $\delta$ ,  
semantic classifier  $M_{\text{sem}}$

**Ensure:** filtered image set  $\mathcal{I}_{\text{filtered}}$

```

1: /* compute emotion accuracy */
2:  $\mathbf{F} \in \mathbb{R}^{m \times c} \leftarrow M_{\text{CLIP}}(\mathcal{I})$ 
3:  $\mathbf{P}_{\text{emo}} \in \mathbb{R}^{m \times 1} \leftarrow M_{\text{emo}}(\mathbf{F})$ 
4: /* compute semantic clarity scores */
5:  $\mathbf{S}_{\text{sem}} \in \mathbb{R}^{m \times 1} \leftarrow M_{\text{sem}}(\mathbf{F})$ 
6: /* sort by emotion accuracy (Emo-A) */
7:  $\mathbf{R}_{\text{emo}} \in \mathbb{R}^m \leftarrow \text{argsort}(\mathbf{P}_{\text{emo}}, \text{dim} = -1)$ 
8: /* sort by semantic clarity (Sem-C) */
9:  $\mathbf{R}_{\text{sem}} \in \mathbb{R}^m \leftarrow \text{argsort}(\mathbf{S}_{\text{sem}}, \text{dim} = -1)$ 
10: /* select images within top  $\eta\%$  to  $\delta\%$  */
11:  $\mathcal{I}_{\text{filtered}} \leftarrow \mathcal{I}(\mathbf{R}_{\text{emo}}[\eta\% : \delta\%] \cap \mathbf{R}_{\text{sem}}[\eta\% : \delta\%])$ 
12: Return:  $\mathcal{I}_{\text{filtered}}$ 
```

---

## IV. EXPERIMENTS

### A. Experiments Settings

**Datasets.** We primarily conduct experiments on two large-scale datasets: 1) **EmoSet** [66] comprises 3.3 million images, with 118,102 meticulously labeled by human annotators. It comprises 8 emotion categories along with diverse attributes,

including brightness, colorfulness, scene type, object class, facial expression, and human action, supporting fine-grained analysis. 2) **The Flickr and Instagram (FI)** [67] dataset is a widely used image emotion dataset. It consists of 22,683 images collected from the Flickr and Instagram platforms, each labeled with one of eight emotional categories.

For additional evaluation, we also test on three smaller datasets: 3) **EmotionROI** [68] contains 1980 emotional images from Flickr. It is annotated with six balanced categories: joy, surprise, anger, disgust, fear, and sadness. 4) **Twitter I** [69] and 5) **Twitter II** [35] are two small datasets collected from Twitter. They have 1269 and 603 images respectively. They only contain two affective states: positive and negative.

**Evaluation Metrics.** Following previous works [16], [70], [71], we employ a diverse set of metrics to evaluate our model’s understanding and generation capabilities. 1) **Accuracy:** Top-1 classification accuracy measures the model’s understanding ability. 2) **FID:** Assesses distributional differences between generated and real images. 3) **Emo-A:** Evaluates alignment between generated images and intended emotions. 4) **Sem-C:** Assesses the clarity of generated image content. 5) **LPIPS:** Measures the diversity of generated emotion-driven images. 6) **Sem-D:** Estimates the richness of content linked to each emotion.

**Comparison Methods and Evaluation Protocols.** 1) **Understanding:** Following previous standard works [72], [70], we evaluate our model on the large-scale EmoSet and FI datasets. We also provide extended comparisons on additional three smaller datasets: EmotionROI, Twitter I, and Twitter II. 2) **Generation:** Emotional image content generation is a newly introduced task in EmoGen [16], with its only comparison benchmark EmoSet. All comparative generation methods are evaluated under the same training dataset (EmoSet) and diffusion architecture for a fair comparison.

**Implementation Details.** Our experiments are implemented in PyTorch and conducted on four NVIDIA L40S GPUs, each with 48GB of memory. In the first stage, we set the batch size to 128 and optimized the understanding component using the AdamW optimizer, with an initial learning rate of 0.0001. The AdamW parameters are configured with  $\beta_1 = 0.9$ ,  $\beta_2 = 0.999$ , and a weight decay of 0.001. In the second stage, we jointly train the entire model with a learning rate of 0.01. During the fusion process, a two-layer MLP with ReLU activation is used to map the various visual representations into the input space of the diffusion model. The pre-trained emotion classifier in the emotional correlation coefficient is composed of two fully connected layers, which are trained on top of frozen CLIP features. Based on experimental results, we set the explicit feedback thresholds  $\eta\%$  and  $\delta\%$  to 20% and 80%, respectively.

### B. Comparison with State-of-the-Art Methods

**Visual Emotion Understanding.** As shown in Tab. I, UniEmo demonstrates consistently superior supervised performance on the large-scale EmoSet and FI datasets. Under the ViT-B/32 backbone, UniEmo attains 83.52% on EmoSet and 85.22% on FI, outperforming strong baselines such as CoCoOp,

TABLE I: Comparison results (%) for **visual emotion understanding task** on the large-scale EmoSet and FI dataset.

Method	Backbone	EmoSet	FI
<i>Visual Instruction Tuning</i>			
BLIP2 [73]	ViT-L/14	46.79	-
InstructBLIP [74]	ViT-L/14	42.20	-
Flamingo [75]	ViT-L/14	29.59	-
LLaVA [76]	ViT-L/14	44.03	-
EmoVIT [70]	ViT-L/14	83.36	-
<i>Supervised Emotion Recognition</i>			
MDAN [37]	ResNet-101	75.75	76.41
CoOp [77]	ViT-B/32	76.19	78.66
CoCoOp [78]	ViT-B/32	80.31	77.46
SimEmotion [79]	ViT-B/32	79.06	80.33
PT-DPC [80]	ViT-B/32	77.13	78.07
MASANet [81]	ViT-B/32	-	79.16
MVP [72]	ViT-B/32	81.92	82.76
<b>UniEmo</b>	ViT-B/32	<b>83.52</b>	<b>85.22</b>
<b>UniEmo</b>	ViT-B/16	<b>84.54</b>	<b>86.34</b>
<b>UniEmo</b>	ViT-L/14	<b>85.30</b>	<b>87.65</b>

TABLE II: Additionally main results for **visual emotion understanding task** on other small datasets.

Method	Backbone	EmotionROI	Twitter I	Twitter II
CoOp [77]	ViT-B/32	68.48	89.05	83.78
CoCoOp [78]	ViT-B/32	71.09	91.63	82.94
PT-DPC [80]	ViT-B/32	69.70	90.94	82.50
SimEmotion [79]	ViT-B/32	70.54	89.76	84.21
MVP [72]	ViT-B/32	71.89	92.03	88.21
<b>UniEmo</b>	ViT-B/32	<b>74.25</b>	<b>93.98</b>	<b>89.94</b>
<b>UniEmo</b>	ViT-B/16	<b>75.57</b>	<b>94.75</b>	<b>90.69</b>
<b>UniEmo</b>	ViT-L/14	<b>76.78</b>	<b>95.63</b>	<b>91.68</b>

which achieves 80.31% and 77.46%, and MVP, which reaches 81.92% and 82.76%, respectively. Notably, the performance gain on FI exceeds seven percentage points over CoCoOp, evidencing the robustness of our approach in cross-domain evaluation. When scaled to larger backbones, UniEmo maintains its advantage: with ViT-B/16, it achieves 84.54% on EmoSet and 86.34% on FI; with ViT-L/14, the performance further improves to 85.30% and 87.65%. This not only surpasses the previous best reported by EmoVIT, which records 83.36% on EmoSet, but also establishes a new state-of-the-art across both benchmarks. These results confirm that the improvements of UniEmo are consistent across backbones and stem from its framework design rather than model size alone.

Evaluations on smaller benchmarks, reported in Tab. II, reveal consistent advantages of UniEmo under the ViT-B/32 backbone. On EmotionROI, UniEmo achieves 74.25%, outperforming CoCoOp at 71.09% and SimEmotion at 70.54%, with an absolute gain of over three points. On Twitter I, UniEmo reaches 93.98%, exceeding CoCoOp (91.63%) and SimEmotion (89.76%), while on Twitter II, it attains 89.94%, surpassing CoCoOp (82.94%) and SimEmotion (84.21%) by notable margins. These results demonstrate that UniEmo delivers consistent improvements of approximately 3–7 percentage points across small-scale benchmarks when compared under the same backbone. Moreover, with larger backbones such as ViT-B/16 and ViT-L/14, UniEmo further pushes performance to 94.75% and 95.63% on Twitter I and up to 91.68% on Twitter II, establishing new state-of-the-art results. Together, these findings highlight UniEmo’s robustness in limited-data

TABLE III: **Zero-shot performance** comparison for **visual emotion understanding task** on the FI dataset. Following the experimental protocol of EmoVIT [70], all methods are pre-trained on the EmoSet dataset, highlighting the generalization capabilities of our UniEmo.

Method	Backbone	Accuracy (%)
BLIP2 [73]	ViT-L/14	57.72
InstructBLIP [74]	ViT-L/14	37.97
Flamingo [75]	ViT-L/14	14.91
LLaVA [76]	ViT-L/14	56.04
EmoVIT [70]	ViT-L/14	68.09
CoOp [77]	ViT-B/32	60.52
CoCoOp [78]	ViT-B/32	61.98
MVP [72]	ViT-B/32	65.73
<b>UniEmo</b>	ViT-B/32	<b>68.32</b>
<b>UniEmo</b>	ViT-B/16	<b>70.05</b>
<b>UniEmo</b>	ViT-L/14	<b>71.22</b>

scenarios and confirm that its gains are not confined to large-scale benchmarks but extend effectively to smaller and more domain-specific datasets.

To further assess cross-dataset generalization, we follow the EmoVIT [70] protocol and conduct zero-shot evaluations on FI, with results summarized in Tab. III. In this setting, all models are pretrained solely on EmoSet without fine-tuning on FI. UniEmo achieves 68.32% with the ViT-B/32 backbone, outperforming MVP by more than two points and slightly surpassing EmoVIT. With the ViT-L/14 backbone, UniEmo reaches 71.22%, setting a new state-of-the-art in zero-shot emotion understanding. These results further demonstrate its robust generalization capability, effectively avoiding dataset-specific biases.

**Visual Emotion Generation.** To evaluate the visual emotion generation capabilities of UniEmo, we perform a fair comparison using the metrics established in EmoGen [16]. The results in Tab. IV demonstrate that UniEmo significantly outperforms existing state-of-the-art methods in the visual emotion generation task across multiple evaluation metrics. UniEmo achieves superior performance in terms of FID, LPIPS, and Emo-A, indicating its ability to generate high-quality, perceptually diverse, and emotion-consistent images. Moreover, the model also excels in Sem-C and Sem-D, showcasing its capacity to produce semantically coherent and rich visual outputs.

In Fig. 5, we qualitatively compare UniEmo with existing generation methods across five emotions. To facilitate intuitive comparisons, we evaluated generated images with consistent semantic themes, *e.g.*, *tigers*, *puppies*, and *lakes*. The final row showcases the outputs from UniEmo, which demonstrate a higher degree of realism and emotional alignment when compared to the preceding methods. Specifically, the generated images by UniEmo are more contextually coherent, with vivid details that effectively convey the target emotions. For example, the tigers in the *anger* category display intense expressions and dynamic postures, while other methods generate images with ambiguous emotional cues. In the *amusement* category, our method generates vibrant, diverse flowers with rich colors and textures, closely matching the intended emotional theme. In contrast, Dreambooth [24] and EmoGen [16] generate more repetitive and less varied flowers. These results demonstrate



TABLE IV: **Performance comparison on visual emotion generation task** on the EmoSet dataset. We follow the settings established in EmoGen [16], where all compared methods are trained on EmoSet and adopt the same architecture (stable-diffusion-v1-5 for SD 1.5 and stable-diffusion-xl-base-1.0 for SD XL).  $\dagger$  denotes results reproduced from the official implementation in EmoGen [16].

Method	Diffusion Architecture	FID $\downarrow$	LPIPS $\uparrow$	Emo-A $\uparrow$	Sem-C $\uparrow$	Sem-D $\uparrow$
Stable Diffusion [21]	SD 1.5	44.05	0.687	70.77%	0.608	0.0199
DreamBooth [24]	SD 1.5	46.89	0.661	70.50%	0.614	0.0178
Textual Inversion [47]	SD 1.5	50.51	0.702	74.87%	0.605	0.0282
EmoGen [16]	SD 1.5	41.60	0.717	76.25%	0.633	0.0335
<b>UniEmo</b>	SD 1.5	<b>27.73</b>	<b>0.793</b>	<b>79.66%</b>	<b>0.640</b>	<b>0.0383</b>
<i>Generalization across Architectures</i>						
Stable Diffusion XL $^\dagger$ [82]	SD XL	41.57	0.721	76.18%	0.628	0.0298
EmoGen $^\dagger$ [16]	SD XL	37.23	0.753	78.92%	0.638	0.0357
<b>UniEmo</b>	SD XL	<b>26.61</b>	<b>0.807</b>	<b>81.74%</b>	<b>0.642</b>	<b>0.0392</b>

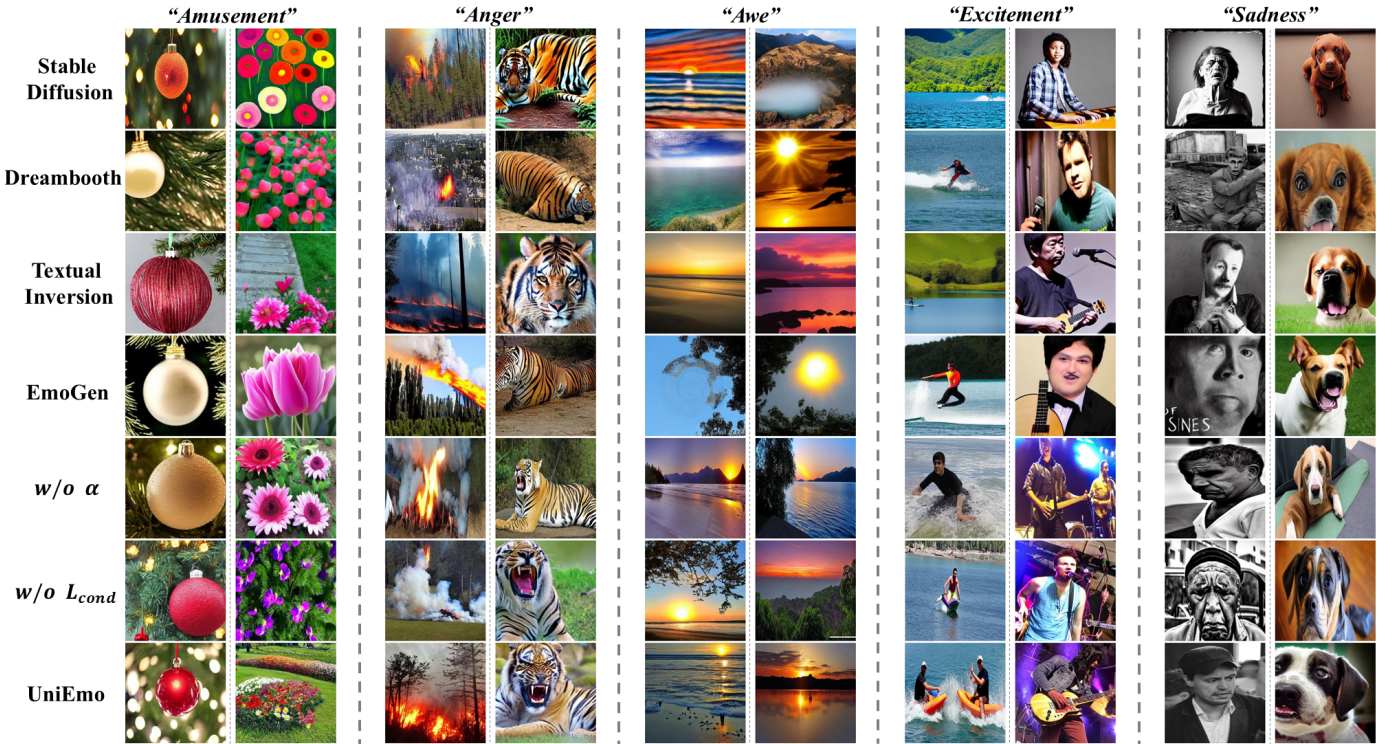


Fig. 5: Qualitative comparison with the state-of-the-art emotional generation methods. To facilitate a more comprehensive comparison, we examine generated images with consistent semantic themes. The settings  $w/o \alpha$  and  $L_{cond}$  represent the results where the emotional correlation coefficient and emotional condition loss are removed, respectively.

UniEmo’s superior ability to generate semantically rich, visually appealing images.

### C. Ablation Study

We primarily conduct ablation studies on the large-scale EmoSet dataset to validate the effectiveness of our different modules.

**The Effect of Expert Query in Visual Emotion Understanding.** As shown in Fig. 6, incorporating expert queries consistently improves the performance. Furthermore, we compare two different integration strategies: 1) **Single-step**, where expert queries are introduced at the input stage, and 2) **Multi-stage**, as proposed in this paper, where expert queries are progressively introduced at different layers. The results demon-

strate that the multi-stage strategy outperforms the single-step, highlighting its superiority in refining feature representations. Additional visualizations are provided in Section IV-D to qualitatively demonstrate the effectiveness of expert queries. Moreover, Fig.7 further explores the impact of query length, suggesting that moderate lengths enhance representation, while overly long queries may introduce complexity.

**Understanding Improves Generation via Expert Queries.** As presented in Tab. V, using the CLs token with two expert queries yields notable performance improvements across multiple metrics. Specifically, the combination of the CLs token with two expert queries shows enhanced results in LPIPS, Emo-A, Sem-C, and Sem-D scores, along with a reduced FID, indicating better quality and diversity in generated images.

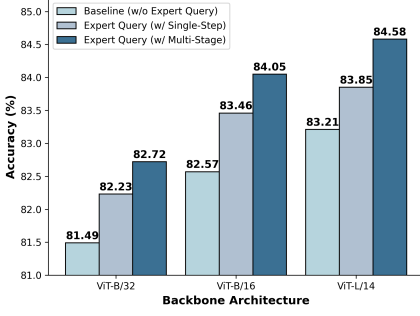


Fig. 6: Ablation study on expert query in visual emotion understanding task across various backbone architectures.

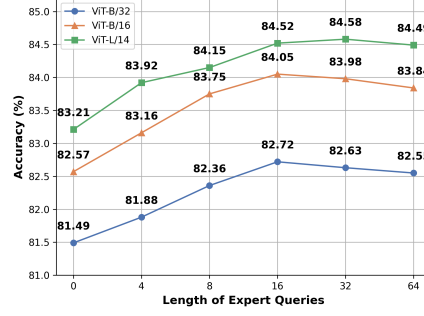


Fig. 7: Ablation study on expert query length in visual emotion understanding task across various architectures.

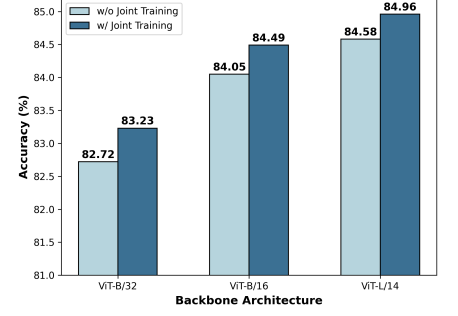


Fig. 8: Ablation study on implicit feedback in visual emotion understanding task across various architectures.

TABLE V: Ablation study on the expert query, emotional correlation coefficient, and emotional condition loss in visual emotion generation. The table evaluates the use of class (Cls), patch (Patch) tokens, and expert queries (Scene and Object). Superscript \* denotes the use of the emotional correlation coefficient.  $L_{ce}$  is cross-entropy loss;  $L_{cond}$  is the proposed emotional condition loss in this paper.

Method	FID ↓	LPIPS ↑	Emo-A ↑	Sem-C ↑	Sem-D ↑
<i>Combination of Expert Query</i>					
Cls	30.02	0.763	71.35%	0.621	0.0331
Cls + Object	29.99	0.769	73.12%	0.625	0.0337
Cls + Scene	30.30	0.771	73.10%	<b>0.627</b>	0.0342
Cls + Patch	29.86	0.764	70.62%	0.617	0.0335
Cls + Object + Scene	<b>29.77</b>	<b>0.775</b>	<b>74.07%</b>	0.625	<b>0.0351</b>
Cls + Patch + Object + Scene	29.83	0.770	72.77%	0.621	0.0339
<i>Emotional Correlation Coefficient</i>					
Cls + Object*	29.21	0.778	75.62%	0.630	0.0352
Cls + Scene*	29.13	0.777	75.44%	0.631	0.0349
Cls + Object* + Scene*	<b>28.56</b>	<b>0.784</b>	<b>77.89%</b>	<b>0.633</b>	<b>0.0358</b>
<i>Emotional Condition Loss</i>					
Cls + Object* + Scene* + $L_{ce}$	28.08	0.787	78.97%	0.635	0.0357
Cls + Object* + Scene* + $L_{cond}$	<b>27.87</b>	<b>0.790</b>	<b>79.77%</b>	<b>0.637</b>	<b>0.0367</b>

These findings indicate that the expert queries effectively capture more nuanced and detailed features, thereby enhancing the model’s generative capabilities.

**The Effect of Emotional Correlation Coefficient and Emotional Condition Loss.** As shown in Tab. V, incorporating the emotional correlation coefficient significantly improves performance under the same token combination. This demonstrates that it improves fusion by emphasizing emotion-relevant features, resulting in more realistic image generation. Additionally, emotional condition loss outperforms standard cross-entropy, notably improving the Emo-A score by better aligning fused features with the target emotion space. Meanwhile, the qualitative analysis in Fig. 5 further illustrates their importance.

**Generation Enhances Understanding via Implicit and Explicit Feedback.** As shown in Fig. 8, joint training in the second stage enhances the model’s understanding by incorporating generation tasks across different backbone architectures. This demonstrates that the generation component provides implicit feedback, optimizing discriminative emotional representations and consistently improving understanding. Furthermore, We conduct the ablation study to evaluate the

effectiveness of the data filtering algorithm as explicit feedback for the understanding component. As shown in Tab. VI, incorporating this filtering mechanism markedly improves the model’s performance in both emotional understanding and generation. Additionally, employing a dual-metric filtering strategy using Emo-A and Sem-C demonstrates superior results, outperforming single-metric approaches by effectively balancing semantic and emotional consistency in the generated output.

**Different Threshold Settings in the Data Filtering Algorithm.** In Table VII, we present an ablation study to evaluate the impact of different threshold settings  $\eta$  and  $\delta$  on the performance of the data filtering algorithm. The baseline method, which lacks explicit feedback, achieves an accuracy of 84.96%, with an FID of 27.87, and a high Emo-A score of 79.77%. However, introducing explicit feedback across various threshold ranges consistently improves several metrics. Notably, the configuration with explicit feedback set between 20% and 80% yields the highest accuracy (85.30%), the lowest FID (27.73), and the best LPIPS score (0.793). Additionally, this configuration achieves the highest scores in Sem-C (0.640) and Sem-D (0.0383), indicating improved semantic consistency and diversity. Although other configurations



TABLE VI: Ablation study on the effectiveness of the data filtering algorithm as explicit feedback. The baseline lacks explicit feedback, while other configurations apply it using different criteria.

Method	Accuracy $\uparrow$	FID $\downarrow$	LPIPS $\uparrow$	Emo-A $\uparrow$	Sem-C $\uparrow$	Sem-D $\uparrow$
Baseline (w/o Explicit Feedback)	84.96%	27.87	0.790	<b>79.77%</b>	0.637	0.0367
Explicit Feedback (w/ Emo-A)	85.10%	27.75	0.781	75.80%	0.611	0.0361
Explicit Feedback (w/ Sem-C)	84.99%	27.93	0.783	75.10%	0.615	0.0380
Explicit Feedback (w/ Emo-A&Sem-C)	<b>85.30%</b>	<b>27.73</b>	<b>0.793</b>	79.66%	<b>0.640</b>	<b>0.0383</b>

TABLE VII: Ablation study on the impact of different threshold settings  $\eta$  and  $\delta$  in the data filtering algorithm.

Method	Accuracy $\uparrow$	FID $\downarrow$	LPIPS $\uparrow$	Emo-A $\uparrow$	Sem-C $\uparrow$	Sem-D $\uparrow$
Baseline (w/o Explicit Feedback)	84.96%	27.87	0.790	<b>79.77%</b>	0.637	0.0367
Explicit Feedback (0 - 100%)	85.17%	27.92	0.778	75.45%	0.623	0.0365
Explicit Feedback (10% - 90%)	85.13%	27.76	0.782	75.71%	0.624	0.0371
Explicit Feedback (50% - 80%)	85.16%	27.96	0.783	76.54%	0.620	0.0370
Explicit Feedback (50% - 100%)	85.05%	27.84	0.775	76.98%	0.625	0.0375
Explicit Feedback (20% - 80%)	<b>85.30%</b>	<b>27.73</b>	<b>0.793</b>	79.66%	<b>0.640</b>	<b>0.0383</b>

TABLE VIII: Ablation Study of the proportion of generated images during training.

Method	Accuracy $\uparrow$	FID $\downarrow$	LPIPS $\uparrow$	Emo-A $\uparrow$	Sem-C $\uparrow$	Sem-D $\uparrow$
5%	85.01%	27.85	0.787	77.56%	0.634	0.0358
10%	85.12%	27.81	0.791	77.91%	0.635	0.0369
20%	85.30%	<b>27.73</b>	<b>0.793</b>	<b>79.66%</b>	<b>0.640</b>	0.0383
30%	<b>85.34%</b>	27.75	0.792	78.34%	0.640	<b>0.0389</b>

also improve performance over the baseline, the 20%-80% setting consistently outperforms them across most metrics. These results suggest that the selection of thresholds  $\eta$  and  $\delta$  within this range allows the algorithm to effectively balance filtering precision and diversity, leading to enhanced overall performance.

#### The Proportion of Generated Images During Training.

In Tab. VIII, we investigated the impact of the proportion of generated images on model performance. Our analysis revealed that varying the percentage of generated images significantly influences key performance metrics. Specifically, we observed that increasing the proportion of generated images generally enhances model accuracy and perceptual quality, as indicated by improvements in metrics such as Accuracy, FID, and LPIPS. However, this improvement comes at the cost of increased computational resources and processing time. After a thorough evaluation, we considered the trade-off between model performance and efficiency. The 20% proportion emerged as a balanced choice, offering a favorable compromise.

#### D. Extended Qualitative Analysis

##### Visualization of the Attention Maps for Expert Queries.

Fig. 9 presents a visualization of the attention maps for expert queries, demonstrating their ability to focus on distinct scene-level and object-level regions associated with various emotional labels. The *Query* first attends to broader contextual areas, such as the concert stage in the *Excitement* image and the natural environment in the *Disgust* image, establishing an initial understanding of the scene that frames the emotional context. Subsequently, the *Object Query* focuses on specific, emotion-evoking details within the images, such as

the flames in the *Anger* image and the bared teeth in the lion’s open mouth in another *Anger* image. This sequential attention mechanism, which progresses from scene-level to object-level extraction, highlights the effectiveness of our hierarchical emotional understanding chain, guided by expert queries. By first attending to the scene and then focusing on key objects, the model progressively refines its understanding of emotional features, supporting the inference of abstract emotional concepts. Leveraging both levels of information enables the model to interpret complex emotional cues and distinguish subtle variations across emotional categories.

**Visualization of the Emotion Transfer.** We further combine emotions with neutral objects to create interesting and meaningful emotional creations, as shown in Fig. 10(a). Each row illustrates the effect of transferring a distinct emotion onto a range of neutral objects, including *Bench*, *Book*, *Cup*, *Lamp*, *Room*, *Sofa*, and *Street*. For example, applying *Amusement* to *Bench* results in a colorful, lively park bench surrounded by vibrant scenery, evoking a cheerful and playful atmosphere, while combining *Amusement* with *Lamp* creates a display of multi-colored, whimsical lighting fixtures. Similarly, transferring *Awe* onto *Room* transforms it into a grandiose space with a breathtaking mountain mural, and applying *Awe* to *Street* produces a scenic, wide-open pathway with inspiring natural surroundings. These transformations highlight the model’s flexibility in generating emotionally rich and contextually appropriate representations by integrating learned emotion features into neutral semantics. With such elements, one can automatically generate images with rich emotional content, enhancing visual storytelling and supporting applications where emotional impact is essential, such as digital art, advertising, and immersive media.

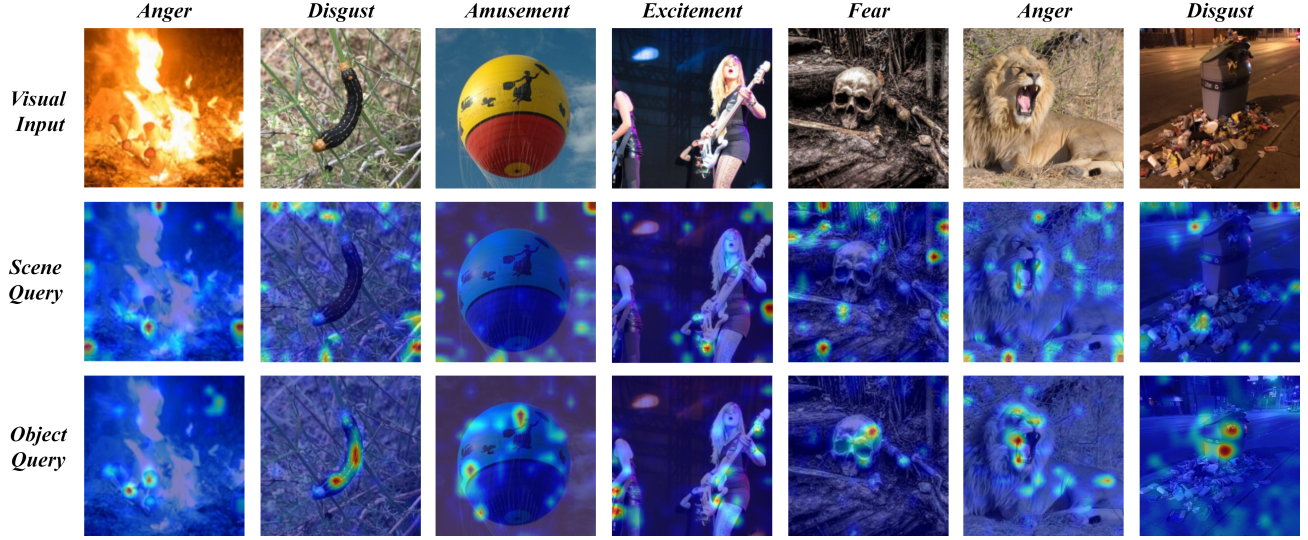


Fig. 9: Visualization of the attention maps for expert queries. It demonstrates that our expert queries can effectively attend to scene and object information within emotional images, respectively.

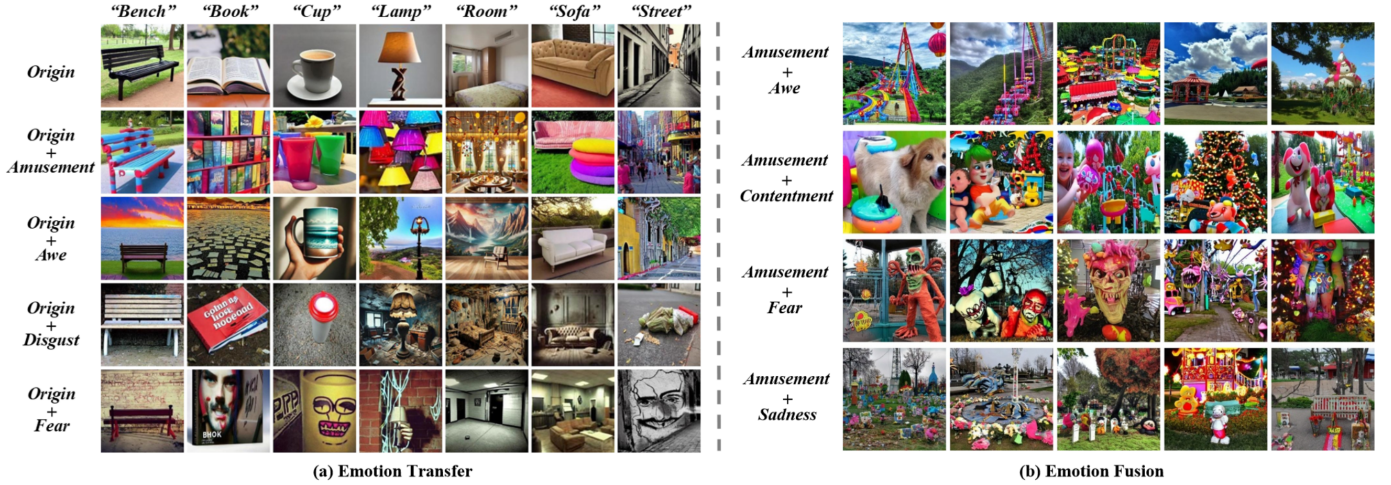


Fig. 10: (a) Emotion transfer, where we combine each of the learned emotion representations with several neutral semantics. With such elements, one can automatically generate images with rich emotional content, enabling a nuanced and expressive visual synthesis. (b) Emotion fusion, where two distinct emotion representations are jointly integrated into the generative process. This allows the model to synthesize images that simultaneously convey both emotions, paving the way for more expressive and contextually rich visual emotion generation.

**Visualization of the Emotion Fusion.** Moreover, to further demonstrate the expressive capacity of our framework, we investigate *emotion fusion*, which synthesizes visual content conditioned on multiple emotional representations simultaneously rather than being restricted to a single label. As shown in Fig. 10(b), such fusion generates complex and nuanced affective imagery that transcends simple emotion transfer. For example, combining *Amusement* with *Awe* produces vibrant and spectacular amusement park scenes, while *Amusement* + *Contentment* yields warm and joyful imagery featuring playful pets and festive decorations. In contrast, fusions such as *Amusement* + *Fear* introduce unsettling or eerie elements into otherwise cheerful contexts, and *Amusement* + *Sadness* results in colorful amusement settings juxtaposed with somber

atmospheres. Beyond producing visually compelling examples, these results highlight the model’s ability to dynamically capture and reconcile distinct affective cues within a single scene. By flexibly adjusting the relative influence of each emotion, the framework can generate outputs ranging from subtle blends to strongly contrasting emotional expressions. This demonstrates that our approach not only enriches the diversity and realism of generated content but also enables fine-grained control over the affective tone of imagery. Such capabilities are particularly valuable for applications that demand nuanced emotional storytelling, including digital art, film production, virtual reality, and advertising. Ultimately, emotion fusion underscores the advantage of our unified framework in moving beyond conventional single-emotion conditioning, paving the

way for more expressive and contextually rich visual emotion generation.

## V. CONCLUSION

In this paper, we introduce UniEmo, a unified framework that integrates emotional understanding with generation. By incorporating learnable expert queries, UniEmo transforms emotional understanding into a coarse-to-fine visual processing chain and conditions a diffusion model to generate emotion-evoking images. To enhance the diversity and fidelity of the generated emotional images, we introduce the emotional correlation coefficient and emotional condition loss into the fusion process. Ultimately, we leveraged UniEmo’s generation capabilities to filter high-quality emotional images, further improving performance. Extensive experiments show that UniEmo significantly outperforms state-of-the-art methods in both emotional understanding and generation tasks.

## REFERENCES

- [1] Z.-Q. Cheng, X. Wu, Y. Liu, and X.-S. Hua, “Video ecommerce++: Toward large scale online video advertising,” *IEEE transactions on multimedia*, vol. 19, no. 6, pp. 1170–1183, 2017.
- [2] —, “Video2shop: Exact matching clothes in videos to online shopping images,” in *Proceedings of the IEEE conference on computer vision and pattern recognition*, 2017, pp. 4048–4056.
- [3] R. Shao, T. Wu, J. Wu, L. Nie, and Z. Liu, “Detecting and grounding multi-modal media manipulation and beyond,” *IEEE Transactions on Pattern Analysis and Machine Intelligence*, 2024.
- [4] R. Shao, T. Wu, and Z. Liu, “Detecting and grounding multi-modal media manipulation,” in *Proceedings of the IEEE/CVF Conference on Computer Vision and Pattern Recognition*, 2023, pp. 6904–6913.
- [5] R. Shao, X. Lan, J. Li, and P. C. Yuen, “Multi-adversarial discriminative deep domain generalization for face presentation attack detection,” in *Proceedings of the IEEE/CVF conference on computer vision and pattern recognition*, 2019, pp. 10023–10031.
- [6] A. Hutchison and L. Gerstein, “Emotion recognition, emotion expression, and cultural display rules: Implications for counseling,” *Journal of Asia Pacific Counseling*, vol. 7, no. 1, 2017.
- [7] J. Yang, J. Li, X. Wang, Y. Ding, and X. Gao, “Stimuli-aware visual emotion analysis,” *IEEE Transactions on Image Processing*, vol. 30, pp. 7432–7445, 2021.
- [8] Y. Lyu, R. Shao, G. Chen, Y. Zhu, W. Guan, and L. Nie, “Puma: Layer-pruned language model for efficient unified multimodal retrieval with modality-adaptive learning,” in *Proceedings of the 33rd ACM International Conference on Multimedia*, 2025.
- [9] H. Zhang, E. Augilius, T. Honkela, J. Laaksonen, H. Gamper, and H. Alene, “Analyzing emotional semantics of abstract art using low-level image features,” in *Advances in Intelligent Data Analysis X*, J. Gama, E. Bradley, and J. Hollmén, Eds. Berlin, Heidelberg: Springer Berlin Heidelberg, 2011, pp. 413–423.
- [10] M. Chen, L. Zhang, and J. P. Allebach, “Learning deep features for image emotion classification,” in *2015 IEEE International Conference on Image Processing (ICIP)*, 2015, pp. 4491–4495.
- [11] X. Zhu, L. Li, W. Zhang, T. Rao, M. Xu, Q. Huang, and D. Xu, “Dependency exploitation: A unified cnn-rnn approach for visual emotion recognition,” in *International Joint Conference on Artificial Intelligence*, 2017. [Online]. Available: <https://api.semanticscholar.org/CorpusID:4963251>
- [12] W. Zhang, X. He, and W. Lu, “Exploring discriminative representations for image emotion recognition with cnns,” *IEEE Transactions on Multimedia*, vol. 22, no. 2, pp. 515–523, 2020.
- [13] B. G. K. Reddy, P. Yashwanthsaai, A. R. Raja, A. Jagarlamudi, N. Leeladhar, and T. T. Kumar, “Emotion recognition based on convolutional neural network (cnn),” in *2021 International Conference on Advancements in Electrical, Electronics, Communication, Computing and Automation (ICAECA)*, 2021, pp. 1–5.
- [14] J. Yang, X. Gao, L. Li, X. Wang, and J. Ding, “Solver: Scene-object interrelated visual emotion reasoning network,” *IEEE Transactions on Image Processing*, vol. 30, pp. 8686–8701, 2021.
- [15] Z. Hu, K. Yuan, X. Liu, Z. Yu, Y. Zong, J. Shi, H. Yue, and J. Yang, “Feallm: Advancing facial emotion analysis in multimodal large language models with emotional synergy and reasoning,” *arXiv preprint arXiv:2505.13419*, 2025.
- [16] J. Yang, J. Feng, and H. Huang, “Emogen: Emotional image content generation with text-to-image diffusion models,” in *2024 IEEE/CVF Conference on Computer Vision and Pattern Recognition (CVPR)*. Los Alamitos, CA, USA: IEEE Computer Society, jun 2024, pp. 6358–6368. [Online]. Available: <https://doi.ieeecomputersociety.org/10.1109/CVPR52733.2024.00608>
- [17] A. Yadollahi, A. G. Shahraki, and O. R. Zaiane, “Current state of text sentiment analysis from opinion to emotion mining,” *ACM Computing Surveys (CSUR)*, vol. 50, no. 2, pp. 1–33, 2017.
- [18] E. Hsieh and B. Nicodemus, “Conceptualizing emotion in healthcare interpreting: A normative approach to interpreters’ emotion work,” *Patient Education and Counseling*, vol. 98, no. 12, pp. 1474–1481, 2015.
- [19] H. Xie, H. Chung, H.-H. Shuai, and W.-H. Cheng, “Learning to prompt for vision-language emotion recognition,” in *2023 11th International Conference on Affective Computing and Intelligent Interaction Workshops and Demos (ACIIW)*. IEEE, 2023, pp. 1–4.
- [20] J. Ho, A. Jain, and P. Abbeel, “Denoising diffusion probabilistic models,” *Advances in Neural Information Processing Systems*, vol. 33, pp. 6840–6851, 2020.
- [21] R. Rombach, A. Blattmann, D. Lorenz, P. Esser, and B. Ommer, “High-resolution image synthesis with latent diffusion models,” in *Proceedings of the IEEE/CVF Conference on Computer Vision and Pattern Recognition*, 2022, pp. 10684–10695.
- [22] P. Dhariwal and A. Nichol, “Diffusion models beat gans on image synthesis,” *Advances in Neural Information Processing Systems*, vol. 34, pp. 8780–8794, 2021.
- [23] L. Zhang, A. Rao, and M. Agrawala, “Adding conditional control to text-to-image diffusion models,” in *Proceedings of the IEEE/CVF International Conference on Computer Vision*, 2023, pp. 3836–3847.
- [24] N. Ruiz, Y. Li, V. Jampani, Y. Pritch, M. Rubinstein, and K. Aberman, “Dreambooth: Fine tuning text-to-image diffusion models for subject-driven generation,” in *Proceedings of the IEEE/CVF Conference on Computer Vision and Pattern Recognition*, 2023, pp. 22500–22510.
- [25] J. Xie, W. Mao, Z. Bai, D. J. Zhang, W. Wang, K. Q. Lin, Y. Gu, Z. Chen, Z. Yang, and M. Z. Shou, “Show-o: One single transformer to unify multimodal understanding and generation,” *arXiv preprint arXiv:2408.12528*, 2024.
- [26] C. Zhou, L. Yu, A. Babu, K. Tirumala, M. Yasunaga, L. Shamsi, J. Kahn, X. Ma, L. Zettlemoyer, and O. Levy, “Transfusion: Predict the next token and diffuse images with one multi-modal model,” *arXiv preprint arXiv:2408.11039*, 2024.
- [27] Y. Wu, Z. Zhang, J. Chen, H. Tang, D. Li, Y. Fang, L. Zhu, E. Xie, H. Yin, L. Yi *et al.*, “Vila-u: a unified foundation model integrating visual understanding and generation,” *arXiv preprint arXiv:2409.04429*, 2024.
- [28] X. Wang, X. Zhang, Z. Luo, Q. Sun, Y. Cui, J. Wang, F. Zhang, Y. Wang, Z. Li, Q. Yu *et al.*, “Emu3: Next-token prediction is all you need,” *arXiv preprint arXiv:2409.18869*, 2024.
- [29] S. Li, J. Xu, J. Wu, M. Xiong, A. Deng, J. Ji, Y. Huang, W. Feng, S. Ding, and B. Hooi, “ID<sup>3</sup>: Identity-Preserving-yet-Diversified Diffusion Models for Synthetic Face Recognition,” *arXiv preprint arXiv:2409.17576*, 2024.
- [30] W. Wang, Q. Sun, F. Zhang, Y. Tang, J. Liu, and X. Wang, “Diffusion feedback helps clip see better,” *arXiv preprint arXiv:2407.20171*, 2024.
- [31] M. Bar, “Visual objects in context,” *Nature Reviews Neuroscience*, vol. 5, no. 8, pp. 617–629, 2004.
- [32] N. H. Frijda, “Emotion experience and its varieties,” *Emotion Review*, vol. 1, no. 3, pp. 264–271, 2009.
- [33] S. Zhao, X. Yao, J. Yang, G. Jia, G. Ding, T.-S. Chua, B. W. Schuller, and K. Keutzer, “Affective image content analysis: Two decades review and new perspectives,” *IEEE Transactions on Pattern Analysis and Machine Intelligence*, vol. 44, no. 10, pp. 6729–6751, 2022.
- [34] J. Lee and E. Park, “Fuzzy similarity-based emotional classification of color images,” *IEEE Transactions on Multimedia*, vol. 13, no. 5, pp. 1031–1039, 2011.
- [35] D. Borth, R. Ji, T. Chen, T. Breuel, and S.-F. Chang, “Large-scale visual sentiment ontology and detectors using adjective noun pairs,” in *Proceedings of the 21st ACM International Conference on Multimedia*, 2013, pp. 223–232.
- [36] J. Machajdik and A. Hanbury, “Affective image classification using features inspired by psychology and art theory,” in *Proceedings of the 18th ACM International Conference on Multimedia*, ser. MM ’10.

- New York, NY, USA: Association for Computing Machinery, 2010, p. 83–92. [Online]. Available: <https://doi.org/10.1145/1873951.1873965>
- [37] L. Xu, Z. Wang, B. Wu, and S. Lui, “Mdan: Multi-level dependent attention network for visual emotion analysis,” in *2022 IEEE/CVF Conference on Computer Vision and Pattern Recognition (CVPR)*, 2022, pp. 9469–9478.
  - [38] T. Rao, X. Li, and M. Xu, “Learning multi-level deep representations for image emotion classification,” *Neural Processing Letters*, vol. 51, pp. 2043–2061, 2020.
  - [39] J. Zhang, M. Chen, H. Sun, D. Li, and Z. Wang, “Object semantics sentiment correlation analysis enhanced image sentiment classification,” *Know-Based Syst.*, vol. 191, no. C, Mar. 2020. [Online]. Available: <https://doi.org/10.1016/j.knsys.2019.105245>
  - [40] D. Borth, T. Chen, R. Ji, and S.-F. Chang, “Sentibank: large-scale ontology and classifiers for detecting sentiment and emotions in visual content,” in *Proceedings of the 21st ACM International Conference on Multimedia*, 2013, pp. 459–460.
  - [41] J. Pan and S. Wang, “Progressive visual content understanding network for image emotion classification,” in *Proceedings of the 31st ACM International Conference on Multimedia*, ser. MM ’23. New York, NY, USA: Association for Computing Machinery, 2023, p. 6034–6044. [Online]. Available: <https://doi.org/10.1145/3581783.3612186>
  - [42] A. Nichol, P. Dhariwal, A. Ramesh, P. Shyam, P. Mishkin, B. McGrew, I. Sutskever, and M. Chen, “Glide: Towards photorealistic image generation and editing with text-guided diffusion models,” *arXiv preprint arXiv:2112.10741*, 2021.
  - [43] A. Ramesh, P. Dhariwal, A. Nichol, C. Chu, and M. Chen, “Hierarchical text-conditional image generation with clip latents,” *arXiv preprint arXiv:2204.06125*, vol. 1, no. 2, p. 3, 2022.
  - [44] Y. Balaji, S. Nah, X. Huang, A. Vahdat, J. Song, Q. Zhang, K. Kreis, M. Aittala, T. Aila, S. Laine, B. Catanzaro, T. Karras, and M.-Y. Liu, “ediff-i: Text-to-image diffusion models with an ensemble of expert denoisers,” 2023. [Online]. Available: <https://arxiv.org/abs/2211.01324>
  - [45] C. Saharia, W. Chan, S. Saxena, L. Li, J. Whang, E. L. Denton, K. Ghasemipour, R. Gontijo Lopes, B. Karagol Ayan, T. Salimans *et al.*, “Photorealistic text-to-image diffusion models with deep language understanding,” *Advances in Neural Information Processing Systems*, vol. 35, pp. 36 479–36 494, 2022.
  - [46] W. Liao, K. Hu, M. Y. Yang, and B. Rosenhahn, “Text to image generation with semantic-spatial aware gan,” in *Proceedings of the IEEE/CVF Conference on Computer Vision and Pattern Recognition*, 2022, pp. 18 187–18 196.
  - [47] R. Gal, Y. Alaluf, Y. Atzmon, O. Patashnik, A. H. Bermano, G. Chechik, and D. Cohen-Or, “An image is worth one word: Personalizing text-to-image generation using textual inversion,” *arXiv preprint arXiv:2208.01618*, 2022.
  - [48] N. Kumari, B. Zhang, R. Zhang, E. Shechtman, and J.-Y. Zhu, “Multi-concept customization of text-to-image diffusion,” in *Proceedings of the IEEE/CVF Conference on Computer Vision and Pattern Recognition*, 2023, pp. 1931–1941.
  - [49] A. Radford, J. W. Kim, C. Hallacy, A. Ramesh, G. Goh, S. Agarwal, G. Sastry, A. Askell, P. Mishkin, J. Clark *et al.*, “Learning transferable visual models from natural language supervision,” in *International Conference on Machine Learning*, 2021, pp. 8748–8763.
  - [50] Y. Wei, Y. Zhang, Z. Ji, J. Bai, L. Zhang, and W. Zuo, “Elite: Encoding visual concepts into textual embeddings for customized text-to-image generation,” *arXiv preprint arXiv:2302.13848*, 2023.
  - [51] J. Yang, J. Feng, W. Luo, D. Lischinski, D. Cohen-Or, and H. Huang, “Emoedit: Evoking emotions through image manipulation,” *arXiv preprint arXiv:2405.12661*, 2024.
  - [52] C. Li *et al.*, “Emotionprompt: Leveraging psychology for large language models enhancement via emotional stimulus (nd). retrieved 1 august 2023.”
  - [53] Y. He, S. Dang, L. Ling, Z. Qian, N. Zhao, and N. Cao, “Emoticafter: Text-to-emotional-image generation based on valence-arousal model,” *arXiv preprint arXiv:2501.05710*, 2025.
  - [54] R. Zhang, R. Shao, G. Chen, K. Zhou, W. Guan, and L. Nie, “Falcon: Resolving visual redundancy and fragmentation in high-resolution multimodal large language models via visual registers,” *arXiv preprint arXiv:2501.16297*, 2025.
  - [55] Q. Ye, H. Xu, J. Ye, M. Yan, A. Hu, H. Liu, Q. Qian, J. Zhang, and F. Huang, “mplug-owl2: Revolutionizing multi-modal large language model with modality collaboration,” in *Proceedings of the IEEE/CVF conference on computer vision and pattern recognition*, 2024, pp. 13 040–13 051.
  - [56] J. Bai, S. Bai, Y. Chu, Z. Cui, K. Dang, X. Deng, Y. Fan, W. Ge, Y. Han, F. Huang *et al.*, “Qwen technical report,” *arXiv preprint arXiv:2309.16609*, 2023.
  - [57] W. Li, B. Hu, R. Shao, L. Shen, and L. Nie, “Lion-fs: Fast & slow video-language thinker as online video assistant,” in *Proceedings of the Computer Vision and Pattern Recognition Conference*, 2025, pp. 3240–3251.
  - [58] G. Chen, L. Shen, R. Shao, X. Deng, and L. Nie, “Lion: Empowering multimodal large language model with dual-level visual knowledge,” in *Proceedings of the IEEE/CVF Conference on Computer Vision and Pattern Recognition*, 2024, pp. 26 540–26 550.
  - [59] N. Carion, F. Massa, G. Synnaeve, N. Usunier, A. Kirillov, and S. Zagoruyko, “End-to-end object detection with transformers,” in *European conference on computer vision*. Springer, 2020, pp. 213–229.
  - [60] F. Locatello, D. Weissenborn, T. Unterthiner, A. Mahendran, G. Heigold, J. Uszkoreit, A. Dosovitskiy, and T. Kipf, “Object-centric learning with slot attention, 2020,” *URL https://arxiv.org/abs*, 2006.
  - [61] Y. Li, H. Xu, Z. Wang, L. Zhang, and J. Sun, “Exploring plain vision transformer backbones for object detection,” in *ECCV*, 2022.
  - [62] S. Zhang, Z. Wang, X. Wang, and J. Sun, “Dino: Detr with improved denoising anchor boxes for end-to-end object detection,” in *ICLR*, 2023.
  - [63] C. Zhou, C. C. Loy, and B. Dai, “Extract free dense labels from clip,” in *European conference on computer vision*. Springer, 2022, pp. 696–712.
  - [64] Y. Rao, W. Zhao, G. Chen, Y. Tang, Z. Zhu, G. Huang, J. Zhou, and J. Lu, “Denseclip: Language-guided dense prediction with context-aware prompting,” in *Proceedings of the IEEE/CVF conference on computer vision and pattern recognition*, 2022, pp. 18 082–18 091.
  - [65] D. Alexey, “An image is worth 16x16 words: Transformers for image recognition at scale,” *arXiv preprint arXiv:2010.11929*, 2020.
  - [66] J. Yang, Q. Huang, T. Ding, D. Lischinski, D. Cohen-Or, and H. Huang, “Emoset: A large-scale visual emotion dataset with rich attributes,” in *Proceedings of the IEEE/CVF International Conference on Computer Vision*, 2023, pp. 20 383–20 394.
  - [67] Q. You, J. Luo, H. Jin, and J. Yang, “Building a large scale dataset for image emotion recognition: The fine print and the benchmarks,” in *Proceedings of the AAAI conference on artificial intelligence*, vol. 30, 2016.
  - [68] K.-C. Peng, A. Sadovnik, A. Gallagher, and T. Chen, “Where do emotions come from? predicting the emotion stimuli map,” in *2016 IEEE international conference on image processing (ICIP)*. IEEE, 2016, pp. 614–618.
  - [69] Q. You, J. Luo, H. Jin, and J. Yang, “Robust image sentiment analysis using progressively trained and domain transferred deep networks,” in *Proceedings of the AAAI conference on Artificial Intelligence*, vol. 29, no. 1, 2015.
  - [70] H. Xie, C.-J. Peng, Y.-W. Tseng, H.-J. Chen, C.-F. Hsu, H.-H. Shuai, and W.-H. Cheng, “Emovit: Revolutionizing emotion insights with visual instruction tuning,” in *Proceedings of the IEEE/CVF Conference on Computer Vision and Pattern Recognition*, 2024, pp. 26 596–26 605.
  - [71] M. Heusel, H. Ramsauer, T. Unterthiner, B. Nessler, and S. Hochreiter, “Gans trained by a two time-scale update rule converge to a local nash equilibrium,” *Advances in Neural Information Processing Systems*, vol. 30, 2017.
  - [72] Q. Xu, Y. Wei, S. Yuan, J. Wu, L. Wang, and C. Wu, “Learning emotional prompt features with multiple views for visual emotion analysis,” *Information Fusion*, vol. 108, p. 102366, 2024.
  - [73] J. Li, D. Li, S. Savarese, and S. Hoi, “Blip-2: Bootstrapping language-image pre-training with frozen image encoders and large language models,” in *International conference on machine learning*. PMLR, 2023, pp. 19 730–19 742.
  - [74] W. Dai, J. Li, D. Li, A. Tiong, J. Zhao, W. Wang, B. Li, P. Fung, and S. Hoi, “Instructblip: towards general-purpose vision-language models with instruction tuning. arxiv,” *Preprint posted online on June*, vol. 15, no. 2023, p. 4, 2023.
  - [75] J.-B. Alayrac, J. Donahue, P. Luc, A. Miech, I. Barr, Y. Hasson, K. Lenc, A. Mensch, K. Millican, M. Reynolds *et al.*, “Flamingo: a visual language model for few-shot learning,” *Advances in neural information processing systems*, vol. 35, pp. 23 716–23 736, 2022.
  - [76] H. Liu, C. Li, Q. Wu, and Y. J. Lee, “Visual instruction tuning,” *Advances in neural information processing systems*, vol. 36, 2024.
  - [77] K. Zhou, J. Yang, C. C. Loy, and Z. Liu, “Learning to prompt for vision-language models,” *International Journal of Computer Vision*, vol. 130, no. 9, pp. 2337–2348, 2022.
  - [78] —, “Conditional prompt learning for vision-language models,” in *Proceedings of the IEEE/CVF conference on computer vision and pattern recognition*, 2022, pp. 16 816–16 825.

- [79] S. Deng, G. Shi, L. Wu, L. Xing, W. Hu, H. Zhang, and Y. Xiang, "Simemotion: A simple knowledgeable prompt tuning method for image emotion classification," in *International Conference on Database Systems for Advanced Applications*. Springer, 2022, pp. 222–229.
- [80] S. Deng, L. Wu, G. Shi, L. Xing, M. Jian, Y. Xiang, and R. Dong, "Learning to compose diversified prompts for image emotion classification," *Computational Visual Media*, pp. 1–15, 2024.
- [81] J. Cen, C. Qing, H. Ou, X. Xu, and J. Tan, "Masanet: Multi-aspect semantic auxiliary network for visual sentiment analysis," *IEEE Transactions on Affective Computing*, 2024.
- [82] D. Podell, Z. English, K. Lacey, A. Blattmann, T. Dockhorn, J. Müller, J. Penna, and R. Rombach, "Sdxl: Improving latent diffusion models for high-resolution image synthesis," *arXiv preprint arXiv:2307.01952*, 2023.